High-Permittivity Conjugated Polyelectrolyte Interlayers for High-Performance Bulk Heterojunction Organic Solar Cells

Jurgen Kesters, Sanne Govaerts, Geert Pirotte, Jeroen Drijkoningen, Michele Chevrier, Niko Van den Brande, Xianjie Liu, Mats Fahlman, Bruno Van Mele, Laurence Lutsen, Dirk Vanderzande, Jean Manca, Sebastien Clement, Elizabeth Von Hauff and Wouter Maes

Original Publication:

Jurgen Kesters, Sanne Govaerts, Geert Pirotte, Jeroen Drijkoningen, Michele Chevrier, Niko Van den Brande, Xianjie Liu, Mats Fahlman, Bruno Van Mele, Laurence Lutsen, Dirk Vanderzande, Jean Manca, Sebastien Clement, Elizabeth Von Hauff and Wouter Maes, High-Permittivity Conjugated Polyelectrolyte Interlayers for High-Performance Bulk Heterojunction Organic Solar Cells, 2016, ACS Applied Materials and Interfaces, (8), 10, 6309-6314.
http://dx.doi.org/10.1021/acsami.6b00242

High Permittivity Conjugated Polyelectrolyte Interlayers for High Performance Bulk Heterojunction Organic Solar Cells

Jurgen Kesters,[†] *Sanne Govaerts,*[†] *Geert Pirotte,*[†] *Jeroen Drijkoningen,*[‡] *Michèle Chevrier,*[§,∥] *Niko Van den Brande,*[¥] *Xianjie Liu,*[¶] *Mats Fahlman,*[¶] *Bruno Van Mele,*[¥] *Laurence Lutsen,*[†,±] *Dirk Vanderzande,*[†,±] *Jean Manca,*[⊥] *Sébastien Clément,*[*,§] *Elizabeth Von Hauff,*[*,δ] *and Wouter Maes*[*,†,±]

[†] Institute for Materials Research (IMO) – Design & Synthesis of Organic Semiconductors (DSOS), Hasselt University, Agoralaan 1 - Building D, B-3590 Diepenbeek, Belgium

[‡] Institute for Materials Research (IMO) – Electrical and Physical Characterization (ELPHYC), Hasselt University, Wetenschapspark 1, B-3590 Diepenbeek, Belgium

[§] Institut Charles Gerhardt, Université de Montpellier, Place Eugène Bataillon, 34095 Montpellier Cedex 05, France

∥ Laboratory for Polymeric and Composites Materials, Center for Innovation in Materials and Polymers, Research Institute for Science and Engineering of Materials, University of Mons – UMONS, 23 Place du Parc, B-7000 Mons, Belgium

[¥] Physical Chemistry and Polymer Science (FYSC), Vrije Universiteit Brussel (VUB), Pleinlaan 2, B-1050 Brussels, Belgium

[¶] Division of Surface Physics and Chemistry, IFM, Linköping University, SE-58183 Linköping, Sweden

[±] IMEC, IMOMEC, Universitaire Campus - Wetenschapspark 1, B-3590 Diepenbeek, Belgium

[⊥] X-LaB, Hasselt University, Agoralaan 1 - Building D, B-3590 Diepenbeek, Belgium

[δ] Physics of Energy, Department of Physics and Astronomy, Vrije Universiteit Amsterdam, De Boelelaan 1105, 1081 HV Amsterdam, The Netherlands

ABSTRACT

Conjugated polyelectrolyte (CPE) interfacial layers present a powerful way to boost the *I-V* characteristics of organic photovoltaics. Nevertheless, clear guidelines with respect to the structure of high-performance interlayers are still lacking. In this work, impedance spectroscopy is applied to probe the dielectric permittivity of a series of polythiophene-based CPE's. The presence of ionic pendant groups grants the formation of a capacitive double layer, boosting the charge extraction and device efficiency. A counteracting effect is the diminishing affinity with the underlying photoactive layer. To balance these two effects, copolymer structures containing non-ionic side chains are found to be beneficial.

KEYWORDS: organic photovoltaics, cathode interlayers, conjugated polyelectrolytes, impedance spectroscopy, dielectric permittivity

Organic photovoltaics (OPV) have demonstrated strong potential as an innovative source of renewable energy, adding appealing features to classical solar cell technology, in particular in terms of architectural freedom (flexibility, reduced weight, color, semi-transparency), low-light performance and low cost (high throughput) large area production.[1-2] Polymer solar cells comprised of intimate blends of conjugated polymers and (methano)fullerenes have recently demonstrated power conversion efficiencies (PCEs or η) exceeding 10% in single junction devices, mainly through extensive structural optimization of the polymer donor material.[3-5] Simultaneously, interface optimization through dedicated interlayer materials has afforded significant enhancements of one or more *I-V* parameters. Conjugated polyelectrolytes (CPEs), conjugated polymers containing multiple ionic moieties, are frequently employed as cathodic or anodic interlayer materials, as the ionic nature allows for processing from orthogonal (eco-friendly) solvents.[6-8] One particular CPE material that stands out is PFN ({[9,9-bis(3'-*N*,*N*-dimethylamino)propyl]2,7-fluorene}-*alt*-2,7-(9,9-dioctylfluorene)), widely used as a powerful interfacial layer with a reported top efficiency of 9.2% when applied in an inverted solar cell stack in combination with PTB7:$PC_{71}BM$.[3] Apart from conjugated polymer based interfaces, alternative organic materials are considered as well, such as the non-conjugated polymer PEIE (polyethylenimine ethoxylated), small molecule and C_{60} derivatives.[9-11]

The detailed working mechanism of the organic interlayers, in particular with respect to the structural properties of the employed materials, is not fully understood at this stage. The generally accepted understanding involves the formation of an interfacial dipole, as demonstrated through Kelvin probe force microscopy (KPFM) or ultraviolet photoelectron spectroscopy (UPS).[8,10] By deposition of a charged species on top of an apolar (active layer) or metallic (electrode) substrate, preferred orientation of the ionic moieties results in a shift in the vacuum level.[12] Other hypotheses comment on the energy level alignment at the organic/metal interface or active layer doping.[13,14] An extensive investigation on the influence of different interlayer materials on top of various substrates was performed by Kemerink *et al.*[15] The proposed mechanism involves the formation of an image charge, causing alterations in the work functions (as determined by KPFM). From these findings, a model was postulated involving the formation of dipoles depending on the ability of the charged constituents to move. Additionally, it was shown that the size of the counter-ion determines the extent to which the work function can be manipulated. No definite translations toward photovoltaic performances were made, however. Continuing from this study, Bao and co-workers recently proposed a general model for energetics at conjugated electrolyte/electrode interfaces, combining the interface dipole step induced by ion migration or side chain electrostatic realignment with equilibration of the Fermi level due to oxidation/reduction of the π-delocalized backbone at the interface as per the 'integer charge transfer' model.[16] They outline how conjugated electrolytes should be designed to achieve the smallest charge injection/extraction barrier combined with optimized charge transport. For thick charge transporting interlayers, donor π-conjugated anionic CPEs and acceptor π-conjugated cationic CPEs are optimal as anode and cathode, respectively, breaking through the current thickness limitation, whereas for thin tunneling interlayers, acceptor π-conjugated anionic CPEs and donor π-conjugated cationic CPEs are optimal as anode and cathode.

In 2011, Bazan *et al*. reported on polythiophene-type cathodic interfacial materials with pendant trimethylammonium groups (P3TMAHT).[17] For standard architecture polymer solar cells based on PCDTBT:$PC_{71}BM$, a PCE of 6.3% was obtained (compared to 5.3% without interlayer). In previous work, we have replaced Bazan's trimethylammonium end groups by imidazolium functionalities.[18] Application of this material as cathodic interlayer in standard architecture

$PCDTBT:PC_{71}BM$ solar cells resulted in a PCE of 6.7%, a clear enhancement in comparison to the reference device (5.7%) and devices with P3TMAHT as interfacial layer (6.5%). In the present work, we have examined a broader array of potential cathode interlayer materials, based on a common polythiophene backbone, but decorated with different pendant side chains bearing various ionic end groups, with the goal to elucidate the underlying mechanism for improved performance (particularly photocurrent). The polythiophene based CPEs clearly belong to the class of thin tunneling donor π-conjugated cationic CPE interlayers.[16] The main advantage of the polythiophene backbone resides in its structural (synthetic) versatility, as copolymer structures are readily obtained with high control over the final composition and topology.

From the range of available CPEs,[19-22] four representative materials were selected, three homopolymers containing imidazolium, pyridinium and phosphonium end groups, as well as a specific random (50/50) copolythiophene with triethylene glycol and imidazolium-substituted hexyl side chains (Figure 1). The corresponding counter-ions were limited to bromide and bis(trifluoromethylsulfonyl)imide (TFSI). As a donor polymer, PBDTTPD (poly[bis(2'-ethylhexyloxy)benzo[1,2-*b*:4,5-*b'*]dithiophene-*alt*-*N*-octylthieno[3,4-*c*]pyrrole-4,6-dione]) (Figure S1) was chosen, which has been reported to deliver PCEs up to 8.3% in combination with $PC_{71}BM$.[23-25]

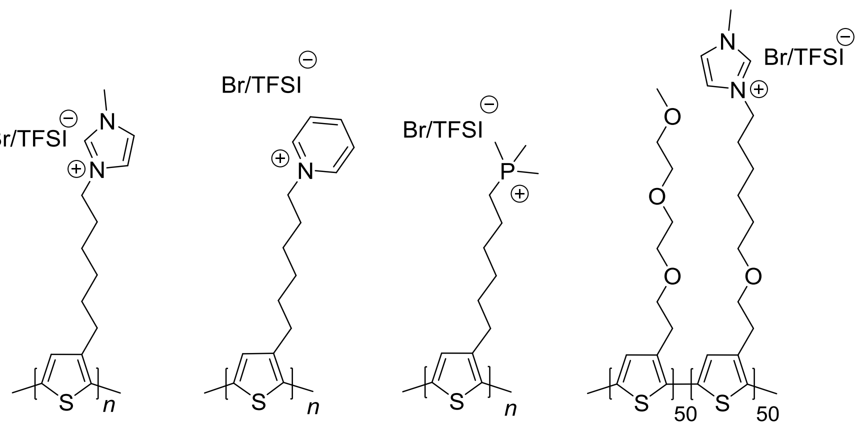

Figure 1. Chemical structures of the employed polythiophene-based conjugated polyelectrolytes **P1−P4**.

The PBDTTPD copolymer (M_n 43 kDa, $Đ$ 2.3) employed in the photoactive layer was prepared by Stille polycondensation in a continuous flow synthesis set-up, allowing more straightforward material upscaling with minimal batch-to-batch variations.[25] Ionic (co)polythiophenes **P1−P4** were prepared according to previously reported procedures (see Supporting Information for the synthesis of **P2,TFSI** and **P3,TFSI**).[19-21] Kumada catalyst transfer polymerization (KCTP) was employed to synthesize bromoalkyl-functionalized polythiophene precursors and subsequent post-polymerization functionalization afforded the ionic derivatives. Finally, the bromide counter-ions were exchanged for more hydrophobic TFSI ions to expand the structural diversity and avoid the hygroscopic features imposed by the Br^- ions (*vide infra*).

Prior to evaluation of the interlayer materials in polymer solar cell devices, rapid heat-cool calorimetry (RHC) analysis was performed on these materials, mainly aiming at the determination of the glass transition temperatures (T_g's) (Figure S10, S11 and Table S2). Exchanging the bromide ion for TFSI resulted in considerably lower T_g's and a strong plasticizing effect was observed. As illustrated in Figure S10, the polythiophene based CPEs containing bromide counter-ions show a strong hygroscopic behavior, indicated by the broad temperature range to remove residual water during the first heating. Considering the formation of dipoles at the interface, the presence of water risks to obscure underlying mechanisms, hindering comparison of the different interfacial materials. Therefore, it was decided to focus on the CPEs containing TFSI counter-ions, for which no hygroscopic character was observed (Figure S10).

To evaluate the effect of the different polythiophene based interlayer materials on device efficiency, bulk heterojunction polymer solar cells with the standard architecture glass/ITO/PEDOT:PSS/PBDTTPD:$PC_{71}BM$/interlayer/Al were prepared. For the photoactive layer (PAL), a total concentration of 20 mg/mL was utilized (1:1.5 polymer:$PC_{71}BM$ ratio) and the reference device employed calcium instead of a CPE, affording an average PCE of 7.3% (with a top efficiency of 7.9%). Polythiophenes **P1−P4,TFSI** were spin-coated on top of the PAL from methanol solutions with optimized concentrations (0.25 mg/mL for **P1−P3,TFSI**, 1 mg/mL for **P4,TFSI**) providing highest efficiencies**.** Table 1 and Figure S12 show the improvements in photovoltaic performance upon incorporation of the cathodic interlayers. The enhanced PCEs can mostly be ascribed to higher short-circuit current densities (J_{sc}). Utilization of **P4,TFSI** resulted in an additional small gain in fill factor (FF), resulting in a top PCE of 9.1% (average 8.2%). A negligible difference between forward and reverse bias was observed and the measurement speed did not significantly alter the *I-V* parameters either. A control device with pure methanol spin-coated on top of the PAL also provided some efficiency increase (7.7% average, 7.9% best PCE), in accordance with previous findings,[17,18] but the obtained values were still significantly below the efficiencies observed upon incorporation of the CPE interlayers. Finally, a reference device without any interlayer (no Ca or CPE) nor methanol treatment was fabricated as well, demonstrating a reduced V_{oc} and FF, similar to past observations.[17,18] The best performing interface material, **P4,TFSI**, was also deposited on top of PCDTBT:$PC_{71}BM$ (1:4

polymer:$PC_{71}BM$ ratio), showing a similar rise in efficiency, but this time strongly affecting all *I*-*V* parameters (Table 1).

Table 1. Photovoltaic performances of PBDTTPD:$PC_{71}BM$ and PCDTBT:$PC_{71}BM$ polymer solar cells with or without the incorporation of cathode interfacial layers.

PAL donor material	Interfacial material	*V*oc [V]	*J*sc [mA/cm^2]	FF	Average η [%][a)]	Best η [%]
PBDTTPD	Ca	0.92 ± 0.00	11.28 ± 0.69	0.71 ± 0.01	7.32 ± 0.20	7.91
PBDTTPD	**P1,TFSI**	0.92 ± 0.00	11.57 ± 0.55	0.70 ± 0.00	7.44 ± 0.38	8.08
PBDTTPD	**P2,TFSI**	0.93 ± 0.01	12.12 ± 0.67	0.70 ± 0.02	7.90 ± 0.41	8.54
PBDTTPD	**P3,TFSI**	0.92 ± 0.01	11.73 ± 0.60	0.71 ± 0.01	7.72 ± 0.37	8.30
PBDTTPD	**P4,TFSI**	0.93 ± 0.01	12.25 ± 0.76	0.72 ± 0.01	8.21 ± 0.51	9.08
PBDTTPD	/	0.88 ± 0.01	11.69 ± 0.11	0.64 ± 0.01	6.49 ± 0.22	6.79
PCDTBT	Ca	0.85 ± 0.01	10.15 ± 0.76	0.53 ± 0.03	4.54 ± 0.37	5.11
PCDTBT	**P4,TFSI**	0.89 ± 0.01	11.55 ± 0.73	0.59 ± 0.03	6.01 ± 0.40	6.42

[a)]Average efficiencies gathered over 16−20 devices.

Ultraviolet photoelectron spectroscopy (UPS) measurements were performed for **P1−P4,TFSI** when deposited on either the applied device stack (without top electrode) or on passivated aluminum films. The work function of the PBDTTPD:$PC_{71}BM$ PAL was determined at 4.66 eV, and upon incorporation of the CPEs, no significant differences between the interlayer materials could be observed, with work functions varying around 4.5−4.7 eV (Figure S13). Alternatively, deposition of the CPEs on top of passivated Al films showed a clear decrease in work function from 3.9 eV for Al to 3.7–3.8 eV for the different interlayers (Figure S14), similar to when employing calcium. No distinct trend among the interlayer series could be determined, however.

To gain insights into the deposition behavior of the CPE materials on top of the PBDTTPD:$PC_{71}BM$ active layer blend and its potential influence on the final photovoltaic performance, atomic force microscopy (AFM) measurements were performed (Figure 2, with the corresponding adhesion images in Figure S15). For a dedicated comparison, all CPE materials were spin-coated from methanol in identical concentrations (0.25 mg/mL). As can be observed, the AFM images clearly demonstrate an incomplete PAL coverage with the formation of stain-like structures. Noteworthy are the strong differences in height-width ratios for the various CPEs, potentially linked with the observed trend in solar cell performance (**P1,TFSI** < **P3,TFSI** < **P2,TFSI** < **P4,TFSI**). For **P1,TFSI** and **P3,TFSI**, the strongest 'dewetting' is observed, with globule heights up to ~30−40 nm. The deposition of **P2,TFSI** occurred slightly more beneficial, with globule thicknesses up to ~18 nm. The increased affinity of **P4,TFSI** (with a slight enhancement in FF and top PCE in comparison with **P1−P3,TFSI**) for the underlying PBDTTPD:$PC_{71}BM$ layer (best height-width ratio of the globules, maximum height ~13 nm) can possibly be ascribed to the copolymer nature of this CPE, with 50% of non-ionic side chains.[26] Furthermore, the active layer coverage of a specific CPE material also differs when processed on top of a different PAL. The coverage of **P4,TFSI** on top of PCDTBT:$PC_{71}BM$ is clearly more homogeneous (Figure S16), possibly identifying the origin of the observed differences in photovoltaic performance enhancement.

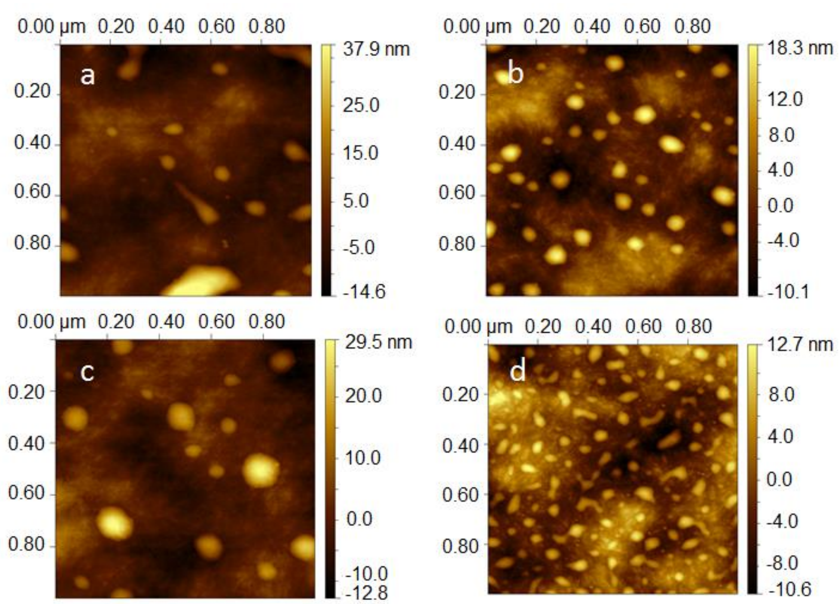

Figure 2. AFM topography images of the polymer solar cells (PBDTTPD:$PC_{71}BM$) based on a) **P1,TFSI**, b) **P2,TFSI**, c) **P3,TFSI**, and d) **P4,TFSI**. The relative area covered by the CPE is 12, 19, 13 and 22% for **P1**–**P4,TFSI**, respectively.

The side chain functionalities on the CPE materials applied in the present study are known to grant an increased dielectric constant (ε). The correlation between the dielectric properties of CPE interlayers and increased solar cell performance has, however, not yet been studied in detail. Enhancement of ε in organic semiconductors is considered to be a key parameter toward OPV performance improvement,[27-33] since it can diminish important loss processes originating from Coulombic interactions between oppositely charged charge carriers. High permittivity materials show lower exciton binding energies and hence recombination decreases, improving the charge carrier extraction efficiency.[34,35] When targeting dielectric permittivity enhancement, activities have so far focused mainly on the photoactive layer materials.[28-33] Nonetheless, concerning dielectric thin films, it was recently demonstrated that incorporation of highly polarizable materials can reduce the surface-charge accumulation at the interface, thereby enhancing the photovoltaic performance in PTB7:$PC_{71}BM$ solar cells.[36]

To confirm the correlation between the high dielectric constants of the interlayer materials and improved solar cell performance, we performed impedance spectroscopy measurements. The **P2,TFSI** and **P4,TFSI** materials were analyzed in detail, as they provided the largest PCE gains. Measurements were performed on both pristine interlayer films in a diode structure (impedance and phase angle spectra in Figure S17). Figure 3a illustrates the real component, permittivity (ε'), and the imaginary component, dielectric loss (ε''), of the complex permittivity as a function of frequency for the pristine interlayer diodes. In the low frequency range (10–10^2 Hz), the permittivity values are large for both **P2,TFSI** ($\varepsilon' \sim 75$) and **P4,TFSI** ($\varepsilon' \sim 50$) and decrease with increasing frequency. The low frequency regime, i.e. approaching DC conditions, is most relevant for understanding solar cell operation. The permittivity values are quite high compared to other values commonly determined for polythiophene derivatives (ε ~ 3 for P3HT).[33,37] The high permittivities of the CPEs are attributed to the ionic end groups of the polymers, which align due the applied electric field to form a capacitive layer. The larger permittivity observed for **P2,TFSI** can be ascribed to the polymer structure. **P2** is a homopolymer, fully decorated with ionic moieties, while **P4** is a statistical copolymer containing only 50% of ionic end groups. The decrease in permittivity with frequency is a result of the finite speed at which the dipoles in the system can follow changes in the applied electric field. At intermediate frequencies (10^2–10^4 Hz), the permittivity of **P2,TFSI** decreases more rapidly with frequency, resulting in lower values than for **P4,TFSI** at frequencies above 10^4 Hz. We additionally observe a feature in the **P2,TFSI** spectrum at frequencies between 10^3–10^4 Hz. Furthermore, the dielectric loss spectra demonstrate higher values of ε'' for **P2,TFSI** than for **P4,TFSI** over the entire spectrum, as well as the occurrence of a peak at 10^4 Hz in the loss tangent ($\varepsilon''/\varepsilon'$) spectrum (Figure S18). Dielectric loss is associated with heat dissipation from dipole reorientation in a changing electric field, and hence the peak at 10^4 Hz in the loss spectrum of **P2,TFSI** can be attributed to losses related to rearrangement of the ionic groups. In contrast, the permittivity of **P4,TFSI** is relatively more constant with frequency and no notable features are observed in the loss spectrum. This indicates that the chemical structure of the copolymer, which includes triethylene glycol pendant groups, leads to a more stable dipole alignment. Finally, at high frequencies (10^5–10^6 Hz), the permittivity of both materials decreases further, as the ionic moieties cannot follow the rapidly changing electric field.[33] Summarizing these results, it is apparent that adding ionic end groups significantly increases the permittivity.

However, the molecular structure is important for controlling ionic orientation and stabilizing the interfacial dipole.

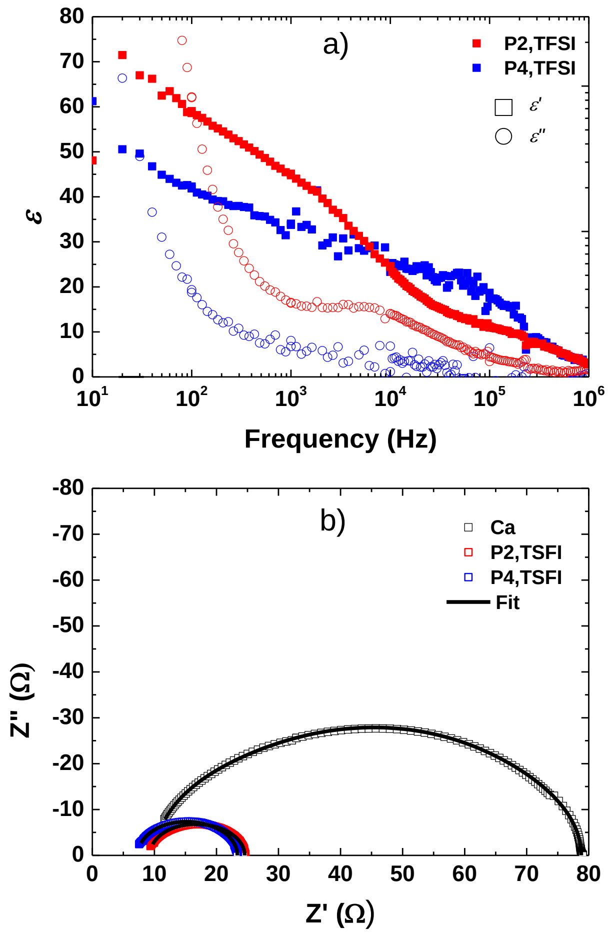

Figure 3. a) Dielectric permittivity (real (ε' – squares) and imaginary (ε'' – circles) components) for pristine interlayer diodes based on **P2,TFSI** and **P4,TFSI**. b) Impedance spectra of the reference PBDTTPD:$PC_{71}BM$ device (black symbols) and solar cells incorporating **P2,TFSI** (red symbols) and **P4, TFSI** (blue symbols) interlayers taken under illumination at a DC offset voltage of 0.9 V. The spectra were fit with an equivalent circuit model (black lines).

To correlate the influence of the high permittivity values of the interlayers with solar cell performance, we performed impedance spectroscopy on the solar cells in the dark and under illumination at a DC voltage offset close to open circuit conditions (0.9 V). In Figure 3b, the illuminated impedance spectra of the reference device and solar cells incorporating **P2,TFSI** and **P4,TSFI** are shown in a Nyquist plot. The spectra were modeled using an equivalent circuit consisting of three resistor-capacitor (RC) elements,[38] and the data from fits are represented in the figure. A detailed description of the equivalent circuit modeling as well as the dark impedance spectra can be found in the Supporting Information. From the real component of the impedance (*Z*'), it can be seen that the total device resistance is highest for the reference device (79 Ω) and considerably lower for the devices incorporating the interlayers (~24 Ω). We observe that the total resistance of the device without the interlayer remains constant between the dark (76.7 Ω) and illuminated (78.8 Ω) measurements. In the case of the devices with the interlayers, a substantial decrease in device resistance is seen (from 52.2 Ω to 24.6 Ω for **P2,TFSI**, and from 46.3 Ω to 23.4 Ω for **P4,TFSI**). Additionally, from the modeling we find that the total device capacitance is a factor of two higher under illumination in solar cells with the interlayers (~ 60 nF) compared to the reference device (28 nF). The increase in capacitance observed in the solar cells cannot be attributed to the high permittivity of the interlayers alone, as the dark measurements reveal only a slight increase in capacitance upon incorporation of the interlayers (from 30 nF to 40 nF). The decrease in device resistivity (i.e. increase in conductivity) and increase in device capacitance under illumination in the solar cells incorporating the interlayers can be associated with increased photocurrent in the active layer.

To evaluate the influence of the transient dielectric properties of the interlayers on the solar cells under short circuit conditions, we performed external quantum efficiency (EQE) measurements. These measurements were performed at low chopper frequencies between 21 and 471 Hz. At these lower frequencies, it is expected that the interlayers have the strongest impact on the photocurrent.

Plotting the integrated current densities as obtained from EQE (J_{EQE}) in function of the chopper frequency revealed a similar trend as observed in Figure 3 (EQE spectra in Figure S20). As illustrated in Figure 4, the J_{EQE} of a reference PBDTTPD:$PC_{71}BM$ device remains almost constant over the entire range of applied frequencies. However, upon incorporation of the CPE interlayers, a pronounced frequency dependence of the J_{EQE} values is observed. Higher values are measured at low chopper frequencies due to a beneficial orientation of the ionic groups on the polythiophene side chains. Increasing the frequency of the chopper leads to a decrease in the extent of preferred ionic orientation, resulting in J_{EQE}'s approaching the reference values. Furthermore, Figure 4 illustrates that the J_{EQE} of the device based on **P4,TFSI** always resides at a higher value than observed for **P2,TFSI**. From the AFM results and the impedance analysis, we believe this to be correlated to the higher coverage of the underlying photoactive layer combined with more beneficial ionic orientation. Even though **P2,TFSI**, containing (relatively) more ionic groups, exhibits a higher potential for capacitive double layer formation, its chemical structure reduces the molecular ordering as well as its affinity for the underlying photoactive layer, consequently reducing its effectiveness in improving device performance. In contrast, **P4,TFSI**, bearing triethylene glycol side chains in combination with ionic pendant groups, allows for both a higher compatibility with the underlying PBDTTPD:$PC_{71}BM$ active layer as well as the formation of a stable capacitive double layer, and therefore a stronger enhancement in PCE.

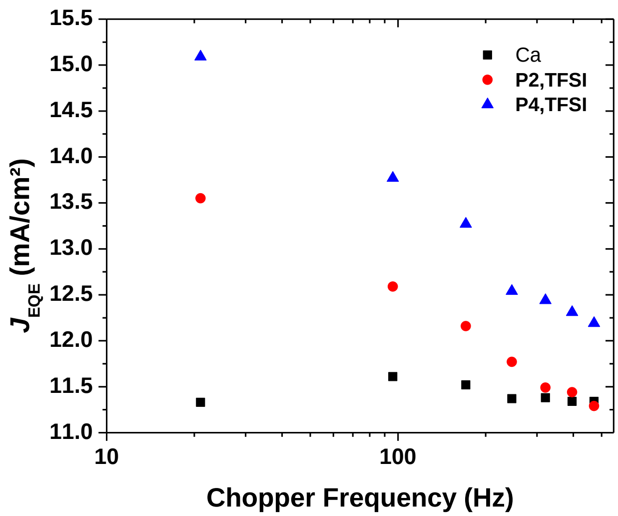

Figure 4. Integrated current densities from the EQE spectra of polymer solar cell devices (PBDTTPD:PC_{71}BM) in function of chopper frequency.

In conclusion, we have demonstrated a considerable improvement in polymer solar cell efficiency upon insertion of polythiophene based cathodic interlayers. Application of copolymer **P4,TFSI** to PBDTTPD:PC_{71}BM solar cells afforded a top efficiency of 9.1% for this photoactive layer (compared to 7.9% for the reference device). Combination of the RHC, UPS, AFM, impedance and EQE data gathered in this study provided deeper insights in the fundamental working principles underpinning improved device performance. With impedance spectroscopy and frequency dependent EQE measurements, the importance of transient measurements for understanding interfacial dipole formation and the corresponding influence on solar cell performance was demonstrated. The achieved insights also allow to formulate some design rules toward optimal (polythiophene based) CPE interlayers. Counter-ions affording hygroscopic materials should be avoided to increase device (efficiency) reproducibility. The presence of ionic pendant groups allows orthogonal processing on top of the photoactive layer and grants the formation of a capacitive double layer, boosting the charge extraction and device efficiency. A counteracting effect is that the material's affinity with respect to the underlying photoactive layer diminishes. To enhance the interlayer-photoactive layer compatibility, copolymer structures containing a certain amount of non-ionic side chains are found to be beneficial. However, traditional alkyl side chains reduce the polarity and can cause solubility issues. In general, a more covering interfacial layer with a retained ability to create a stable capacitive double layer will grant strongest performance enhancement. Further efforts on copolymer structures with different monomer compositions[19-21] have been initiated to support the hypotheses formulated and to optimize OPV device performance.

ASSOCIATED CONTENT

Supporting Information

The Supporting Information (chemical structure of the donor material, experimental data and NMR spectra of **P2,TFSI** and **P3,TFSI**, cyclic voltammetry data, thermal analysis, solar cell data, UPS, AFM, impedance data and EQE spectra) is available free of charge via the Internet at http://pubs.acs.org.

AUTHOR INFORMATION

Corresponding Authors

*E-mail: wouter.maes@uhasselt.be
*E-mail: sebastien.clement1@umontpellier.fr
*E-mail: e.l.von.hauff@vu.nl

ACKNOWLEDGEMENTS

This work was supported by the IAP 7/05 project 'Functional Supramolecular Systems', granted by the Science Policy Office of the Belgian Federal Government (BELSPO). We are also grateful for financial support by the Research Program of the Research Foundation – Flanders (FWO) (project G.0415.14N) and by the Foundation for Fundamental Research on Matter (FOM) (V0714M-13MV60) from the Netherlands Organization for Scientific Research (NWO). Hasselt University and IMEC are partners within the Solliance network, the strategic alliance for research and development in the field of thin-film PV energy in the Eindhoven-Leuven-Aachen region. X. L. acknowledges support from The Swedish Research Council Linnaeus grant LiLi-NFM at Linköping University. N.V. thanks the Vrije Universiteit Brussel (VUB) for a postdoctoral grant. TA Instruments is acknowledged for the RHC equipment. S.C. and M.C. thank the University of Montpellier, the CNRS and the University of Mons for financial support.

REFERENCES

(1) Cao, W.; Xue, J. Recent Progress in Organic Photovoltaics: Device Architecture and Optical Design. *Energy Environ. Sci.* **2014**, *7*, 2123–2144.

(2) Mazzio, K. A.; Luscombe, C. K. The Future of Organic Photovoltaics. *Chem. Soc. Rev.* **2015**, *44*, 78–90.

(3) He, Z.; Zhong, C.; Su, S.; Xu, M.; Wu, H.; Cao, Y. Enhanced Power-Conversion Efficiency in Polymer Solar Cells Using an Inverted Device Structure. *Nat. Photonics* **2012**, *6*, 593–597.

(4) Subbiah, J.; Purushothaman, B.; Chen, M.; Qin, T.; Gao, M.; Vak, D.; Scholes, F. H.; Chen, X.; Watkins, S. E.; Wilson, G. J.; Holmes, A. B.; Wong, W. W. H.; Jones, D. J. Organic Solar Cells Using a High-Molecular-Weight Benzodithiophene-Benzothiadiazole Copolymer with an Efficiency of 9.4%. *Adv. Mater.* **2015**, *27*, 702–705.

(5) Nielsen, C. B.; Ashraf, R. S.; Treat, N. D.; Schroeder, B. C.; Donaghey, J. E.; White, A. J. P.; Stingelin, N.; McCulloch, I. 2,1,3-Benzothiadiazole-5,6-Dicarboxylic Imide – A Versatile Building Block for Additive- and Annealing-Free Processing of Organic Solar Cells with Efficiencies exceeding 8%. *Adv. Mater.* **2015**, *27*, 948–953.

(6) He, Z.; Zhong, C.; Huang, X.; Wong, W.-Y.; Wu, H.; Chen, L.; Su, S.; Cao, Y. Simultaneous Enhancement of Open-Circuit Voltage, Short-Circuit Current Density, and Fill Factor in Polymer Solar Cells. *Adv. Mater.* **2011**, *23*, 4636–4643.

(7) Liu, S.; Zhang, K.; Lu, J.; Zhang, J.; Yip, H.-L.; Huang, F.; Cao, Y. High-Efficiency Polymer Solar Cells via the Incorporation of an Amino-Functionalized Conjugated Metallopolymer as a Cathode Interlayer. *J. Am. Chem. Soc.* **2013**, *135*, 15326–15329.

(8) Lee, B. H.; Jung, I. H.; Woo, H. Y.; Shim, H.-K.; Kim, G.; Lee, K. Multi-Charged Conjugated Polyelectrolytes as a Versatile Work Function Modifier for Organic Electronic Devices. *Adv. Funct. Mater.* **2014**, *24*, 1100–1108.

(9) Ouyang, X.; Peng, R.; Ai, L.; Zhang, X.; Ge, Z. Efficient Polymer Solar Cells Employing a Non-Conjugated Small-Molecule Electrolyte. *Nat. Photonics* **2015**, *9*, 520–524.

(10) Vasilopoulou, M.; Douvas, A. M.; Georgiadou, D. G.; Constantoudis, V.; Davazoglou, D.; Kennou, S.; Palilis, L. C.; Daphnomili, D.; Coutsolelos, A. G.; Argitis, P. Large Work Function Shift of Organic Semiconductors Inducing Enhanced Interfacial Electron Transfer in Organic Optoelectronics Enabled by Porphyrin Aggregated Nanostructures. *Nano Res.* **2014**, *7*, 679–693.

(11) O'Malley, K. M.; Li, C.-Z.; Yip, H.-L.; Jen, A. K.-Y. Enhanced Open-Circuit Voltage in High Performance Polymer/Fullerene Bulk-Heterojunction Solar Cells by Cathode Modification with a C_{60} Surfactant. *Adv. Energy Mater.* **2012**, *2*, 82–86.

(12) Seo, J. H.; Yang, R.; Brzezinski, J. Z.; Walker, B.; Bazan, G. C.; Nguyen, T.-Q. Electronic Properties at Gold/Conjugated-Polyelectrolyte Interfaces. *Adv. Mater.* **2009**, *21*, 1006–1011.

(13) Braun, S.; Salaneck, W. R.; Fahlman, M. Energy-Level Alignment at Organic/Metal and Organic/Organic Interfaces. *Adv. Mater.* **2009**, *21*, 1450–1472.

(14) Li, C.-Z.; Chueh, C.-C.; Ding, F.; Yip, H.-L.; Liang, P.-W.; Li, X.; Jen, A. K.-Y. Doping of Fullerenes via Anion-Induced Electron Transfer and its Implication for Surfactant Facilitated High Performance Polymer Solar Cells. *Adv. Mater.* **2013**, *25*, 4425–4430.

(15) van Reenen, S.; Kouijzer, S.; Janssen, R. A. J.; Wienk, M. M.; Kemerink, M. Origin of Work Function Modification by Ionic and Amine-Based Interface Layers. *Adv. Mater. Interfaces* **2014**, *1*, 1400189.

(16) Bao, Q.; Liu, X.; Wang, E.; Fang, J.; Gao, F.; Braun, S.; Fahlman, M. Regular Energetics at Conjugated Electrolyte/Electrode Modifier for Organic Electronics and their Implications on Design Rules. *Adv. Mater. Interfaces* **2015**, *2*, 1500204.

(17) Seo, J. H.; Gutacker, A.; Sun, Y.; Wu, H.; Huang, F.; Cao, Y.; Scherf, U.; Heeger, A. J.; Bazan, G. C. Improved High-Efficiency Organic Solar Cells via Incorporation of a Conjugated Polyelectrolyte Interlayer. *J. Am. Chem. Soc.* **2011**, *133*, 8416–8419.

(18) Kesters, J.; Ghoos, T.; Penxten, H.; Drijkoningen, J.; Vangerven, T.; Lyons, D. M.; Verreet, B.; Aernouts, T.; Lutsen, L.; Vanderzande, D.; Manca, J.; Maes, W. Imidazolium-Substituted Polythiophenes as Efficient Electron Transport Materials Improving Photovoltaic Performance. *Adv. Energy Mater.* **2013**, *3*, 1180–1185.

(19) Rubio-Magnieto, J.; Thomas, A.; Richeter, S.; Mehdi, A.; Dubois, P.; Lazzaroni, R.; Clément, S.; Surin, M. Chirality in DNA-π Conjugated Polymer Supramolecular Structures: Insights into the Self-Assembly. *Chem. Commun.* **2013**, *49*, 5483–5485.

(20) Ghoos, T.; Brassinne, J.; Fustin, C.-A.; Gohy, J.-F.; Defour, M.; Van den Brande, N.; Van Mele, B.; Lutsen, L.; Vanderzande, D. J.; Maes, W. Imidazolium-Substituted Ionic (Co)Polythiophenes: Compositional Influence on Solution Behavior and Thermal Properties. *Polymer* **2013**, *54*, 6293–6304.

(21) Ghoos, T.; Malinkiewicz, O.; Conings, B.; Manca, J.; Lutsen, L.; Vanderzande, D.; Bolink, H. J.; Maes, W. Solution-Processed Bi-Layer Polythiophene-Fullerene Organic Solar Cells. *RSC Adv.* **2013**, *3*, 25197–25203.

(22) Zilberberg, K.; Behrendt, A.; Kraft, M.; Scherf, U.; Riedl, T. Ultrathin Interlayers of a Conjugated Polyelectrolyte for Low Work-Function Cathodes in Efficient Inverted Organic Solar Cells. *Org. Electron.* **2013**, *14*, 951–957.

(23) Cabanetos, C.; El Labban, A.; Bartelt, J. A.; Douglas, J. D.; Mateker, W. M.; Fréchet, J. M. J.; McGehee, M. D.; Beaujuge, P. M. Linear Side Chains in Benzo[1,2-*b*:4,5-*b'*]dithiophene-Thieno[3,4-*c*]pyrrole-4,6-dione Polymers Direct Self-Assembly and Solar Cell Performance. *J. Am. Chem. Soc.* **2013**, *135*, 4656–4659.

(24) Bartelt, J. A.; Douglas, J. D.; Mateker, W. R.; El Labban, A.; Tassone, C. J.; Toney, M. F.; Fréchet, J. M. J.; Beaujuge, P. M.; McGehee, M. D. Controlling Solution-Phase Polymer Aggregation with Molecular Weight and Solvent Additives to Optimize Polymer-Fullerene Bulk Heterojunction Solar Cells. *Adv. Energy Mater.* **2014**, *4*, 1301733.

(25) Pirotte, G.; Kesters, J.; Verstappen, P.; Govaerts, S.; Manca, J.; Lutsen, L.; Vanderzande, D.; Maes, W. Continuous Flow Polymer Synthesis toward Reproducible Large-Scale Production for Efficient Bulk Heterojunction Organic Solar Cells. *ChemSusChem* **2015**, *8*, 3228–3233.

(26) Oh, S.-H.; Na, S.-I.; Jo, J.; Lim, B.; Vak, D.; Kim, D.-Y. Water-Soluble Polyfluorenes as an Interfacial Layer Leading to Cathode-Independent High Performance of Organic Solar Cells. *Adv. Funct. Mater.* **2010**, *20*, 1977–1983.

(27) Koster, L. J. A.; Shaheen, S. E.; Hummelen, J. C. Pathways to a New Efficiency Regime for Organic Solar Cells. *Adv. Energy Mater.* **2012**, *2*, 1246–1253.

(28) Lu, Y.; Xiao, Z.; Yuan, Y.; Wu, H.; An, Z.; Hou, Y.; Gao, C.; Huang, J. Fluorine Substituted Thiophene-Quinoxaline Copolymer to Reduce the HOMO Level and Increase the Dielectric Constant for High Open-Circuit Voltage Organic Solar Cells. *J. Mater. Chem. C.* **2013**, *1*, 630–637.

(29) Camaioni, N.; Po, R. Pushing the Envelope of the Intrinsic Limitation of Organic Solar Cells. *J. Phys. Chem. Lett.* **2013**, *4*, 1821–1828.

(30) Jahani, F.; Torabi, S.; Chiechi, R. C.; Koster, L. J. A.; Hummelen, J. C. Fullerene Derivatives with Increased Dielectric Constants. *Chem. Commun.* **2014**, *50*, 10645–10647.

(31) Yang, P.; Yuan, M.; Zeigler, D. F.; Watkins, S. E.; Lee, J. A.; Luscombe, C. K. Influence of Fluorine Substituents on the Film Dielectric Constant and Open-Circuit Voltage in Organic Photovoltaics. *J. Mater. Chem. C.* **2014**, *2*, 3278–3284.

(32) Torabi, S.; Jahani, F.; Van Severen, I.; Kanimozhi, C.; Patil, S.; Havenith, R. W. A.; Chiechi, R. C.; Lutsen, L.; Vanderzande, D. J. M.; Cleij, T. J.; Hummelen, J. C.; Koster, L. J. A. Strategy for Enhancing the Dielectric Constant of Organic Semiconductors without Sacrificing Charge Carrier Mobility and Solubility. *Adv. Funct. Mater.* **2015**, *25*, 150–157.

(33) Donaghey, J. E.; Armin, A.; Burn, P. L.; Meredith, P. Dielectric Constant Enhancement of Non-Fullerene Acceptors via Side-Chain Modification. *Chem. Commun.* **2015**, *51*, 14115–14118.

(34) Leblebici, S. Y.; Chen, T. L.; Olalde-Velasco, P.; Yang, W.; Ma, B. Reducing Exciton Binding Energy by Increasing Thin Film Permittivity: An Effective Approach to Enhance Exciton Separation Efficiency in Organic Solar Cells. *Appl. Mater. Interfaces* **2013**, *5*, 10105–10110.

(35) Cho, N.; Schlenker, C. W.; Knesting, K. M.; Koelsch, P.; Yip, H.-L.; Ginger, D. S.; Jen, A. K.-Y. High-Dielectric Constant Side-Chain Polymers Show Reduced Non-Geminate Recombination in Heterojunction Solar Cells. *Adv. Energy Mater.* **2014**, *4*, 1301857.

(36) Hsiao, Y.-C.; Zang, H.; Ivanov, I.; Xu, T.; Lu, L.; Yu, L.; Hu, B. Dielectric Interface Effects on Surface Charge Accumulation and Collection towards High-Efficiency Organic Solar Cells. *J. Appl. Phys.* **2014**, *115*, 154506.

(37) Knipper, M.; Parisi, J.; Coakley, K.; Waldauf, C.; Brabec, C. J.; Dyakonov, V. Impedance Spectroscopy on Polymer-Fullerene Solar Cells. *Z. Naturforsch., A: Phys. Sci.* **2007**, *62*, 490–494.

(38) Guerrero, A.; Montcada, N. F.; Ajuria, J.; Etxebarria, I.; Pacios, R.; Garcia-Belmonte, G.; Palomares, E. Charge Carrier Transport and Contact Selectivity Limit the Operation of PTB7-Based Organic Solar Cells of Varying Active Layer Thickness. *J. Mater. Chem. A* **2013**, *1*, 12345–12354.

TABLE OF CONTENTS GRAPHIC